Naval Research Laboratory

Washington, DC 20375-5320

NRL/MR/7632--19-9856

Coupling Models of the Thermosphere with Lower Atmospheric Numerical Weather Prediction Systems

McArthur Jones, Jr.

Douglas P. Drob

David E. Siskind

John P. McCormack

Sarah E. McDonald

Kenneth F. Dymond

Geospace Science and Technology Branch
Space Sciences Division

Astrid Maute

High Altitude Observatory
National Center for Atmospheric Research
Boulder, CO

February 7, 2019

REPORT DOCUMENTATION PAGE

Form Approved
OMB No. 0704-0188

1. REPORT DATE *(DD-MM-YYYY)*	2. REPORT TYPE	3. DATES COVERED *(From - To)*
07-02-2019	Memorandum Report	10/30/2017 - 10/29/2019

4. TITLE AND SUBTITLE

Coupling Models of the Thermosphere with Lower Atmospheric Numerical Weather Prediction Systems

5a. CONTRACT NUMBER

5b. GRANT NUMBER

5c. PROGRAM ELEMENT NUMBER
NISE

6. AUTHOR(S)

McArthur Jones Jr., Douglas Drob, David Siskind, John McCormack, Austird Maute,*
Sarah McDonald and Kenneth Dymond

5d. PROJECT NUMBER

5e. TASK NUMBER

5f. WORK UNIT NUMBER
76-2N4N-08-5

7. PERFORMING ORGANIZATION NAME(S) AND ADDRESS(ES)

Naval Research Laboratory
4555 Overlook Avenue, SW
Washington, DC 20375-5344

8. PERFORMING ORGANIZATION REPORT NUMBER

NRL/MR/7632--19-9856

9. SPONSORING / MONITORING AGENCY NAME(S) AND ADDRESS(ES)

Naval Research Laboratory
4555 Overlook Avenue, SW
Washington, DC 20375-5344

10. SPONSOR / MONITOR'S ACRONYM(S)

NRL-NISE

11. SPONSOR / MONITOR'S REPORT NUMBER(S)

12. DISTRIBUTION / AVAILABILITY STATEMENT

DISTRIBUTION STATEMENT A: Approved for public release; distribution is unlimited.

13. SUPPLEMENTARY NOTES

*High Altitude Observatory, National Center for Atmospheric Research, P.O. Box 3000, Boulder, CO 80307-3000
Work Performed Under NRL Karles Fellowship

14. ABSTRACT

In this report we analyze the effects two different approaches of constraining a middle and upper atmospheric general circulation model have on accurately reproducing the middle and upper atmospheric variability induced by the 2010 sudden stratospheric warming event. Numerical experiments were performed using the National Center for Atmospheric Research thermosphere-ionosphere-mesosphere-electrodynamics general circulation model (TIME-GCM) constrained by middle atmospheric winds and temperatures from a high-altitude version of the Navy Global Environmental Model (NAVGEM-HA). Model comparisons focused on zonal mean winds, composition, and atmospheric solar tides in the thermosphere-ionosphere system. We found that implementing different methods of constraint produce differences in the simulated dynamics of mesosphere and lower thermosphere, the consequences of which have adverse effects on simulating the peak ionospheric electron density.

15. SUBJECT TERMS

Thermosphere, Ionosphere, Sudden Stratospheric Warming, Newtonian Relaxation, 4D Tendency Nudging, TIME-GCM, NAVGEM-HA

16. SECURITY CLASSIFICATION OF:			17. LIMITATION OF ABSTRACT	18. NUMBER OF PAGES	19a. NAME OF RESPONSIBLE PERSON
a. REPORT	b. ABSTRACT	c. THIS PAGE			McArthur Jones Jr.
Unclassified Unlimited	Unclassified Unlimited	Unclassified Unlimited	Unclassified Unlimited	16	19b. TELEPHONE NUMBER *(include area code)* (202) 767-6317

This page intentionally left blank.

CONTENTS

FIGURES

TABLES

EXECUTIVE SUMMARY

This report presents research conducted by Jones et al. under his Karles Fellowship tenure at NRL. Lower atmospheric meteorology drives up to half of the variability of the thermosphere and ionosphere via propagating waves of various scales that alter the dynamics and composition of the mesosphere, thermosphere, and ionosphere. Recent advancements in middle and upper atmospheric modeling have led to self-consistent, coupled numerical models of the global middle and upper atmosphere, including the ionosphere that can generally incorporate the day-to-day variability in lower and middle atmospheric wave activity by constraining the relevant dynamical fields using observational and/or reanalysis datasets. However, recent studies have found that implementing the established "specified dynamics" (SD) form of Newtonian relaxation (or more commonly referred to as nudging) for constraining middle atmospheric dynamics in the National Center Atmospheric Research (NCAR) thermosphere-ionosphere-mesosphere-electrodynamics general circulation model (TIME-GCM) has produced unusually strong zonal mean zonal winds in the mesosphere and lower thermosphere. Thus, we evaluate in detail the impact that the established SD nudging technique and the recently implemented four-dimensional (4D) tendency nudging technique has on the thermosphere-ionosphere variability. As a case study, we compare TIME-GCM simulations of the 2010 sudden stratospheric warming (SSW) using the two aforementioned nudging techniques, and find that implementing SD and 4D Tendency nudging in the TIME-GCM leads to different SSW induced thermosphere-ionosphere variability. Results presented herein indicate that 4D Tendency nudging has the added potential to improve physics based diagnostic capabilities of model parameters that contribute to data-model differences during the 2010 SSW.

This page intentionally left blank.

COUPLING MODELS OF THE THERMOSPHERE WITH LOWER ATMOSPHERIC NUMERICAL WEATHER PREDICTION SYSTEMS

1. INTRODUCTION

During the past two decades, there has been a paradigm shift from a mainly solar forced upper atmosphere (e.g., thermosphere-ionosphere, TI) to an upper atmosphere that is also subjected to persistent forcing from lower atmospheric meteorology [1,2]. It is now widely recognized that a major source of TI variability is driven by a rich spectrum of upward propagating atmospheric tides, gravity, and planetary waves. Improved knowledge is needed on how the TI is perturbed by tides, gravity, and planetary waves to address the DoD/Navy long-term need of environmental predication of space effects for tactical planning purposes, as well as the maximization of DoD HF and Space systems performance through adaption to the variable environment [3].

In order to better reproduce (and eventually forecast) the short-term (days to weeks) TI variability, observational and/or reanalysis datasets are incorporated into global physics-based numerical models of the stratosphere, mesosphere, thermosphere, and ionosphere to constrain lower and middle atmospheric meteorology. Typically, reanalysis datasets are incorporated via Newtonian relaxation [e.g., 4] or nudging, where model fields are relaxed towards reanalysis fields following a user-specified time constant. Previous results by *Pedatella et al.* [5] have suggested that different upper atmospheric models produce different results, when constrained using different nudging schemes, different data sources, and different altitudes constrained.

The standard nudging approach used in the whole atmospheric and middle-upper atmospheric modeling communities is referred to as "specified dynamics" (SD, see [4,6]). Different implementations of SD nudging have been reported (e.g., the NCAR thermosphere-ionosphere-electrodynamics general circulation model (TIME-GCM by [7]), but the differing effects on model physics have not been quantified. For example, both *Maute et al.* [8] and *Wang et al.* [9] have recently reported zonal mean zonal wind discontinuities in the low-latitude mesopause region in TIME-GCM when incorporating "reanalysis" data via SD nudging.

A somewhat different nudging approach that was originally pioneered by the tropospheric mesoscale modeling community [10], referred to herein as four-dimensional (4D) Tendency nudging, was used by [11] to investigate tidal vertical transport effects on atomic oxygen (O) in the TI. This nudging approach relaxes the model state towards the reanalysis state by adding an artificial tendency term to the prognostic model equation.

In this report, the impact that SD and 4D Tendency nudging have on accurately reproducing the TI variability associated with 2010 sudden stratospheric warming (SSW) event is evaluated. Thus, a set of numerical experiments with the TIME-GCM were performed that constrained the meteorological fields in the stratosphere and mesosphere using NAVGEM-HA (Navy Global Environmental Model a high-altitude version, [12]), from January to late March of 2010. TIME-GCM simulations constrained by NAVGEM-HA winds and temperatures based on the SD nudging approaches of *Maute et al.* [8] and *Wang et al.* [9] (hereafter referred to as M15 and W17, respectively) are presented and compared with those that employed 4D Tendency nudging (hereafter referred to as J18). Comparisons between the different model simulations provide a means to quantify the effects different nudging schemes have on the simulating the zonal mean winds and wave perturbations of the mesosphere and thermosphere that drive much of the TI variability observed during SSW events.

Manuscript approved February 7, 2019.

2. MODEL SIMULATIONS, DATASETS, AND APPROACH

2.1 TIME-GCM

The NCAR TIME-GCM is three-dimensional time-dependent general circulation models designed to self-consistently simulate the circulation, temperature, composition, and electrodynamics of the mesosphere and TI system on a regular grid in spherical coordinates in longitude and latitude, and log-pressure in the vertical assuming hydrostatic balance. The horizontal resolution of the TIME-GCM is 2.5° x 2.5° (longitude x latitude) and 4 grid points per vertical scale height, extending from ~30 km to 450-600 km (depending on solar cycle conditions). For a more detailed description of the TIME-GCM, including its historical development, solar forcing and geomagnetic specifications, and gravity wave parameterization the reader is referred to [8,13,14,15,16]. Of specific interest for this work is the lower boundary forcing. Typically, the model is driven at the lower boundary with zonal and daily averaged reanalysis data and climatological tidal perturbations [17,18]. However, *Maute et al.* [8] later reported problems in simulating the 2010 SSW period by simply forcing the model with realistic meteorological conditions solely at the lower boundary. They instead suggested constraining the dynamical and temperature structure of the stratosphere and mesosphere via nudging to reanalysis data during the boreal winter months of 2010.

2.2 NAVGEM-HA

NAVGEM-HA is a prototype high-altitude numerical weather prediction system designed to study the meteorology of the lower and middle atmosphere from the surface to 100 km. NAVGEM-HA replaces the earlier Navy Operational Global Atmospheric Prediction System-Advanced Level Physics High Altitude forecast model [NOGAPS-ALPHA, 19]. Unlike the earlier NOGAPS-ALPHA system which used a 3-dimensional variational (3DVAR) data assimilation algorithm that consolidates observations within a 6-hour window, the hybrid 4-dimensional variational (4DVAR) NRL data assimilation system (i.e., NAVDAS-AR) in NAVGEM-HA accounts for time-varying observations within the 6-hour window. Specifically, the data assimilation component of NAVGEM-HA produces global synoptic analyses of key meteorological variables (e.g., winds, temperature, geopotential height, water vapor, and ozone) every 6 hours (00, 06, 12, and 18 UTC), which are then used to initialize short term forecasts to produce a combined 3-hourly analysis/forecast product each day. The advantage of this 3-hour cadence is that it allows for a better representation of the prominent wave components responsible for driving much of the TI variability. Additionally, NAVGEM-HA system was recently validated by *McCormack et al.* [12] with multiple independent ground-based MF radar wind observations over the 2009-2010 and 2012-2013 northern hemisphere winters.

2.3 SPECIFIED DYNAMICS (SD) NUDGING IN THE TIME-GCM

SD nudging in the TIME-GCM was implemented to constrain modeled horizontal winds and neutral temperatures at each model time step over a user-specified pressure range by relaxing to a reanalysis field. The SD nudging approaches of M15 and W17 were slightly different (M15 only nudged the longitude and time mean fields, while W17 nudged the full 4-dimensional fields), but in both cases SD nudging was implemented to study the lower atmospheric driving of the mesosphere and lower thermosphere (MLT) and TI. Specifically, the zonal and meridional winds and neutral temperatures in the momentum and thermodynamic energy equations at every model grid point within the nudging domain take the following form:

$$X = (1 - \alpha\zeta(z))X_{Model} + \alpha\zeta(z)X_{Data}, \quad (1)$$

where z = log-pressure level, X_{Model} represents the zonal (u), and meridional (v) winds, and neutral temperature (T) from TIME-GCM and constraining data source (X_{Data}). $\zeta(z)$ is a vertical weighting

function that determines how strongly the model and data source are coupled as a function of log-pressure (or altitude, ultimately defining the nudging domain), and the fraction α is used to determine the relaxation time (i.e., the nudging strength). For example, $\alpha = 1$ means that model fields are overwritten by data fields at each model time step, and do not enter the prognostic equation weighted against model calculated tendency terms, as is the case when $\alpha < 1$.

2.4 4D TENDENCY NUDGING IN THE TIME-GCM

4D Tendency nudging dynamically adjusts model horizontal winds and temperatures to reanalysis data (or observations in the case of data assimilation) by adding an artificial source term to the prognostic zonal, meridional, and thermodynamic energy equations. The correction term is proportional to the difference between the modeled and "observed" states. In this manner, the nudging process acts as a representative proxy for the unresolved model processes, including underlying biases in the free-running model configuration, as well as uncertainties in the parameterized model physics.

Following the mathematical formulation present in *Jeuken et al.* [20] for lower atmospheric models, the relaxation of an atmospheric variable, *X*, to the "observed" state is written as

$$\frac{\partial X}{\partial t} = F_{Model}(X) + G\zeta(z)\,(X_{Model} - X_{Data}) \tag{2}$$

where X_{Model} can be, for example, TIME-GCM horizontal winds and or neutral temperatures. $F_{Model}(X)$ represents model tendency terms (e.g., advection, pressure gradient, gravity wave drag, etc.) in the horizontal momentum and energy equations and the entire second term is the relaxation term (artificial tendency term) whose magnitude is proportional to *G*, the relaxation factor. One distinguishing characteristic (and potential advantage) of 4D Tendency nudging is that it accounts for data-model differences on the right-hand side of the prognostic equations, where M15 and W17 SD-like approaches correct the prognostic variables of interest prior to model calculations of important dynamical processes (including advection, pressure gradients, etc.).

Table 1 — Nomenclature for TIME-GCM Simulations

Label	Reference	Nudging Scheme	Relaxation Time (in hours)
M15	[8]	SD – Zonal Mean	8.33×10^{-3} h
W17	[9]	SD – Full Field	
J18	[28]	4D Tendency	1.85 h

2.5 TIME-GCM SIMULATIONS

To isolate the effects of SD and 4D Tendency nudging schemes on MLT and TI dynamics and composition during the 2010 SSW period (i.e., 3 December 2009 to 21 March 2010), we performed three otherwise identical TIME-GCM simulations. The lower boundary conditions (i.e., zonally/longitudinally and diurnally averaged fields plus tides in u, v, T, and geopotential heights) were specified at log-pressure level -17 using 3-hourly NAVGEM-HA output from *McCormack et al.* [12]. Also in all cases, we used the observed external solar and geomagnetic forcing. The differences between these three TIME-GCM simulations are summarized in Table 1. The M15 (W17) simulation is designed to diagnose the SD nudging approach of *Maute et al.* [9] (*Wang et al.* [9]), i.e., TIME-GCM zonal mean (full field) horizontal winds and neutral temperatures are constrained using 3-hourly NAVGEM-HA zonal mean (full) fields in stratosphere and mesosphere. The J18 simulation is representative of the 4D Tendency nudging approach, where TIME-GCM

zonal mean and wave perturbations in horizontal winds and neutral temperatures are relaxed to 3-hourly NAVGEMHA fields in the middle atmosphere. To minimize any differences in the vertical weighting distribution of the NAVGEM-HA nudging the M15, W17, and J18 TIME-GCM simulations all invoked the same vertical weighting function $\zeta(z)$, such that $\zeta(z)$ equaled 1 at the lower boundary (~30 km), 0.5 at ~70 km, and 0 at ~96 km.

3. RESULTS AND DISCUSSION

3.1 ZONAL MEAN WINDS

The short-term variability in the TI resulting from SSWs is mainly attributed to variability in upward propagating waves, the structures of which are dependent upon the zonal mean wind field of the middle and upper atmosphere through which they propagate [21]. To systematically evaluate the effect that the M15, W17, and J18 nudging schemes have on the zonal mean zonal winds in the TIME-GCM, Figure 1 shows the simulated zonal and diurnal mean zonal winds averaged from 1 January to 21 March 2010.

Figure 1 clearly shows the key differences in mesospheric zonal winds between the three TIME-GCM simulations, specifically at tropical latitudes above ~0.01 hPa. While M15 and W17 reproduce the NAVGEM-HA winds up to the top nudging level, they then both reveal a very sharp jump in the winds to a strong (>50 m s^{-1}) eastward jet immediately above. This sharp vertical gradient was also seen by *Maute et al.* [8] and *Wang et al.* [9] for other SSW events. By contrast, the J18 simulation has a much broader region of strong eastward equatorial winds without the sharp jump at the nudging boundary.

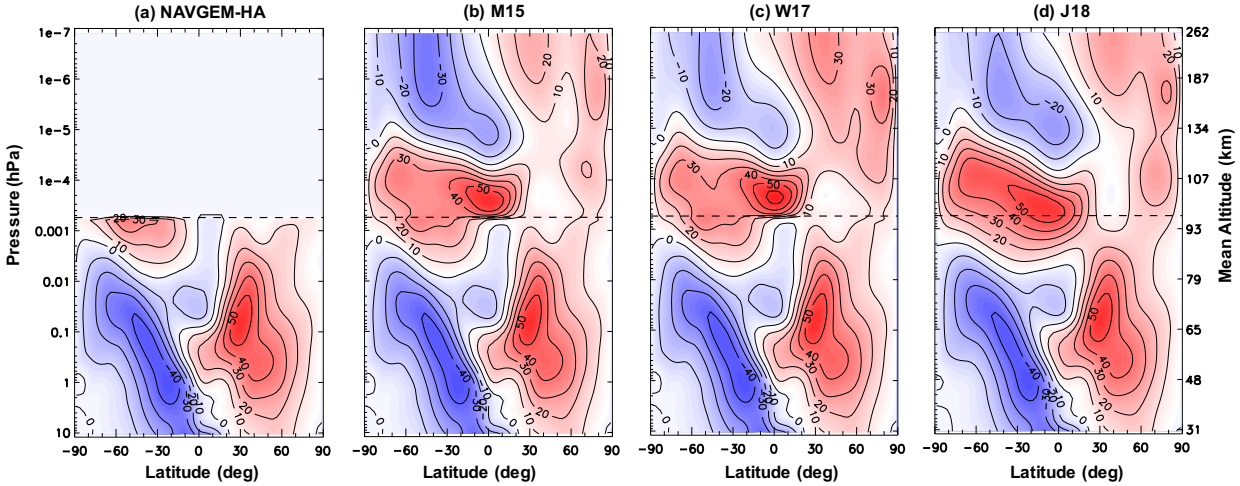

Fig. 1 — Zonal mean zonal winds averaged from 1 January to 21 March 2010 as a function of latitude and pressure/mean altitude simulated by NAVGEM-HA, TIME-GCM M15 (b), W17 (c), and J18 (d). The bold dashed line indicates where $\zeta(z) = 0$, below (above) which the TIME-GCM is constrained (free running) in the M15, W17, and J18 cases. Contours are shown every ±10 m s^{-1}.

Analyzing the mean zonal wind tendencies revealed strong eastward accelerations due to gravity wave drag (on the order of 200 m s^{-1} day^{-1}, not shown) in the M15 and W17 cases. Zonal mean zonal wind tendencies in the J18 case vary smoothly with height through the vertical domain of the TIME-GCM with only moderate gravity wave drag accelerations (~75 m s^{-1} day^{-1}, not shown) calculated. This smoothly varying gravity wave drag is balanced by the artificial tendency term calculated in the 4D Tendency nudging scheme. This is a key characteristic (and potential advantage) of 4D Tendency

nudging, which isolated the essential differences between TIME-GCM and NAVGEM-HA, as at least partially due to differences in gravity wave forcing or propagation at tropical MLT altitudes.

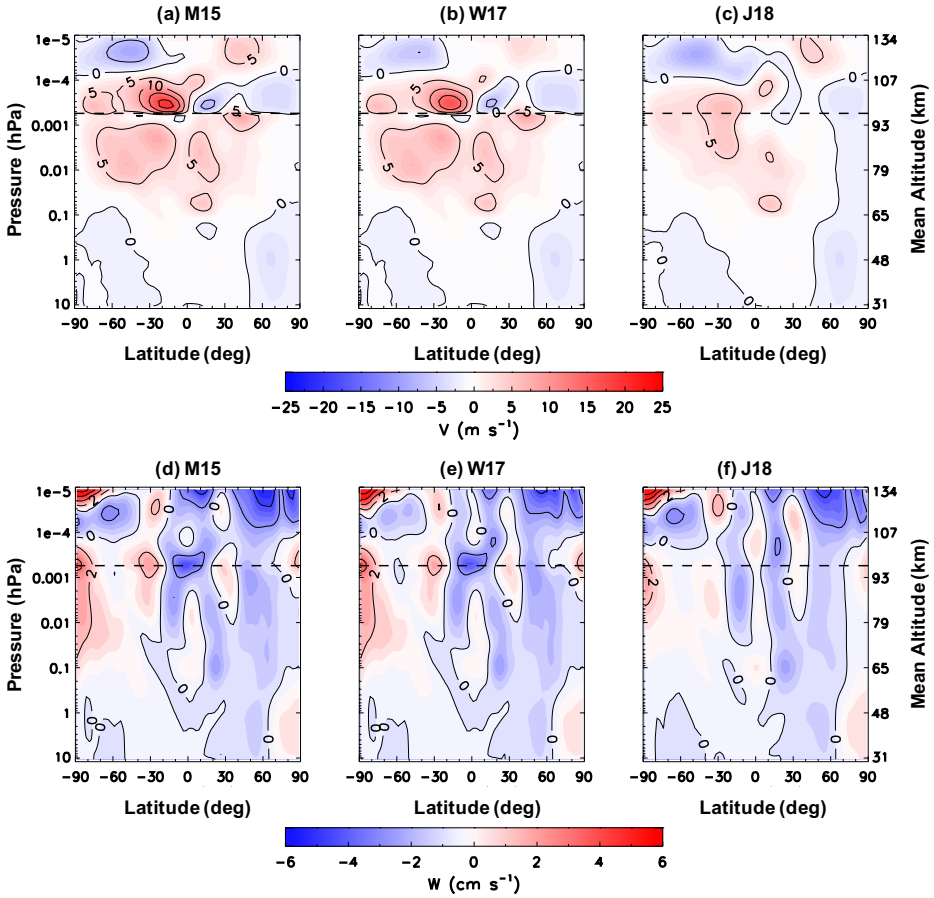

Fig. 2 — Zonal mean meridional (a-c) and vertical (d-f) winds averaged from 1 January to 21 March 2010 as a function of latitude and pressure/mean altitude simulated by TIME-GCM M15 (a,d), W17 (b,e), and J18 (c, f). Meridional (Vertical) winds are contoured every ±5 m s^{-1} (±2 cm s^{-1}). The bold dashed line indicates where $\zeta(z) = 0$, below (above) which the TIME-GCM is constrained (free running) in the M15, W17, and J18 cases.

Figure 2 shows the zonal mean meridional (top row) and vertical (bottom row) winds from our M15, W17, and J18 simulations averaged from 1 January to 21 March 2010. Analogous to the average zonal mean zonal winds, the zonal mean meridional winds in the M15 and W17 simulations exhibit a strong increase at pressure levels immediately above the nudging boundary. Northward winds at tropical southern latitudes reach up to 20 m s^{-1}, while southward winds at tropical northern latitudes reach −8 m s^{-1} in the M15 and W17 simulations (Figures 2a and 2b). This average convergence of meridional winds over the equator, coupled with the strong eastward winds depicted in Figure 1 produce comparatively strong downwelling in the M15 and W17 simulations, with average vertical winds of −3 cm s^{-1} during the boreal winter months (Figures 2d and 2e). In the J18 case, average meridional winds evolve smoothly with altitude across the nudging boundary, with weaker wind speeds (i.e., reaching up to ~8 m s^{-1} at low latitudes Figure 2c). Consequently, weaker convergence/divergence of average zonal and meridional winds leads to weaker vertical winds in Figure 2f at equatorial latitudes in the MLT region. Since the zonal mean meridional circulation in the MLT region can have profound effects on TI composition [e.g., 22], this implies that the differences shown here may have consequences on the calculated compositional morphology of the TI system.

3.2 THE MIGRATING DIURNAL TIDE

Given the documented role planetary waves and tides play in coupling day-to-day lower and middle atmospheric variability to short-term TI variability [e.g., 23] it is important to understand how SD and 4D Tendency nudging differentially affect the vertical wave spectrum in light of the results presented in Section 3.1. Figure 3 shows the migrating (i.e., westward propagating) diurnal tide with zonal wave number 1 (DW1) zonal wind amplitude variability averaged over equatorial latitudes (i.e., ±10º) from NAVGEM-HA and the different TIME-GCM simulations. In general, considering first the zonal winds, the vertical variation of DW1 in the J18 case is smoother than in either M15 or W17 where discontinuities are seen at the nudging boundary. This sharp increase in DW1 zonal wind amplitudes are a by-product of the sharp vertical gradients in the zonal mean zonal winds depicted in Figure 2. Vertical profiles of DW1 mean and daily zonal wind amplitudes from J18 track NAVGEM-HA and smoothly transition across the nudging boundary with a mean amplitude of 10 m s^{-1}.

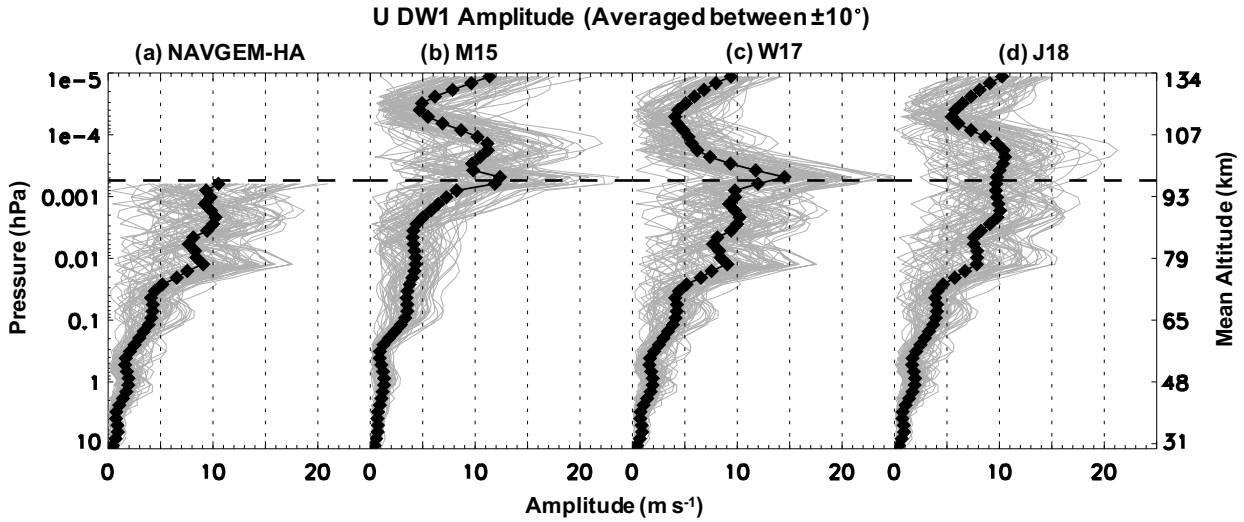

Fig. 3 — Vertical profiles of the DW1 daily (grey) and mean (black-diamonds) zonal wind amplitude averaged between ±10º latitude from 1 January to 21 March 2010 from (a) NAVGEM-HA, TIME-GCM M15 (b), W17 (c), and J18 (d). The bold dashed line indicates where $\zeta(z) = 0$, below (above) which the TIME-GCM is constrained (free running) in the M15, W17, and J18 cases.

There are also subtler differences between the three cases; for example, the amplitude of DW1 in the M15 case in the upper mesosphere (~0.01 hPa) is considerably smaller (near 5 m s^{-1}) than in either the other two cases or in NAVGEM-HA. In general, the W17 case comes closest to matching NAVGEM-HA which is not surprising since both zonal mean and wave fields are tightly coupled to NAVGEM-HA. However, unlike J18, it suffers from the aforementioned sharp discontinuity when nudging stops. Above ~96 km, simulated DW1 zonal wind amplitudes decrease up to ~107 km and then increase again reaching ~10 m s^{-1} due to in-situ absorption of extreme ultraviolet radiation by O_2. It is not immediately evident why the three cases differ in simulating DW1; however, it is clear that different nudging techniques can lead to different tidal behavior up into the lower thermosphere. As will be shown below, these differences can have important ionospheric consequences.

3.3 IMPLICATIONS FOR TI COMPOSITION

Neutral dynamics in the MLT region can have important effects on thermospheric atomic oxygen (O). Subsequently, these effects can propagate up to higher altitudes via molecular diffusion and impact the ionosphere. Given the previously presented zonal mean and tidal results, analyzing the

effects SD and 4D Tendency nudging have on the simulated variability of O in the mesosphere and thermosphere, as well as electron densities in the F-region ionosphere is warranted.

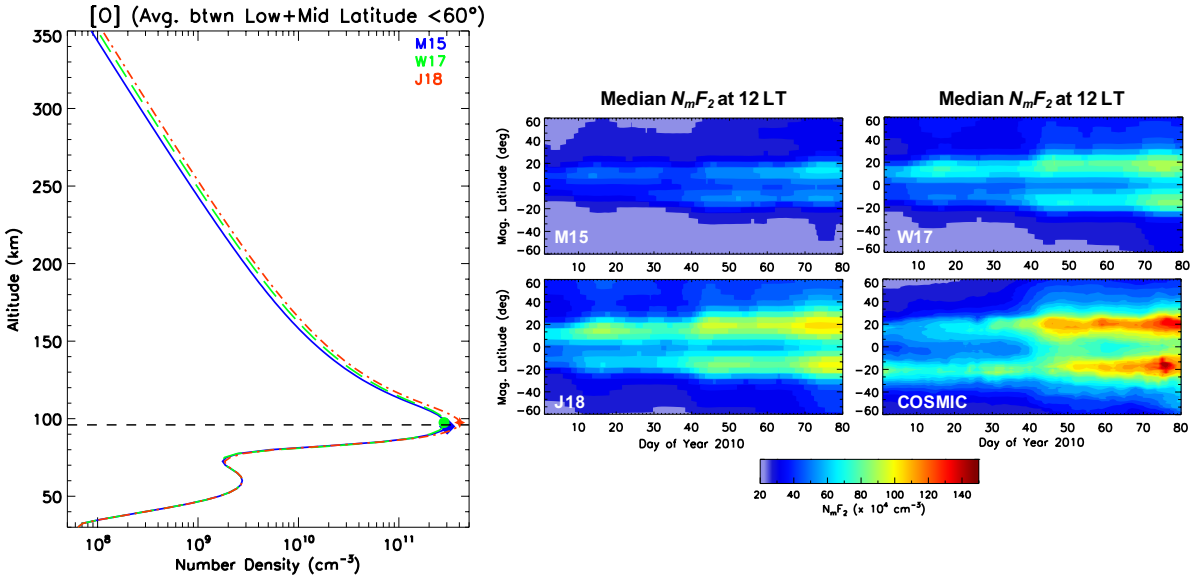

Fig. 4 — Vertical profile of [O] averaged from 1 January to 21 March 2010 and over geographic low and middle latitudes (i.e., ±60º) from M15 (blue), W17 (green), and J18 (red) TIME-GCM simulations. Median local noon (12 LT ± 1.5 h in local time) N_mF_2 values from M15 (top left), W17 (top right), and J18 (bottom left) TIME-GCM simulations, and (bottom right) COSMIC observations as function of day of year in 2010 and magnetic latitude. The grey bold dashed line indicates where $\zeta(z) = 0$, below (above) which the TIME-GCM is constrained (free running) in the M15, W17, and J18 cases. The different symbols mark the maximum [O] value in the different TIME-GCM simulations.

Figure 4 illustrates the effects of different nudging approaches on the simulated mean O number density ([O]) at low and middle latitudes over the period of study. Above ~85 km, M15 (blue), W17 (green), and J18 (red) TIME-GCM simulated average [O] values are different, with J18 [O] being larger than M15 and W17. Specifically, O peak densities of ~4 × 10^{11} cm^{-3} are simulated in the J18 case, while M15 and W17 O peak densities are ~2-3 x 10^{11} cm^{-3} (or ~40% lower). Figure 4 also reveals that the peak [O] simulated by TIME-GCM is sensitive to the nudging technique employed to constrain the model dynamics. Above the [O] peak, molecular diffusion timescales become very rapid, and each simulated [O] profile decreases following its own scale height via the barometric law. As a result, J18 simulated [O] remains approximately ~10-30% higher than M15 and W17 simulated [O].

The cause of the differences in modeled O abundances are likely the differences in mean meridional circulation and tidal transport at the nudging boundary (i.e. near the peak in O concentration). In turn, these differences arise from some of the discontinuities, including the enhanced downward vertical winds and DW1 amplitudes at the nudging boundary, seen in the M15 and W17 cases that are relatively absent in the J18 simulation. The aggregate affect is lower [O] values in the M15 and W17 simulations due to "nudging-induced" increased zonal mean meridional/vertical and DW1 tidal transport, as more O is transported downward into the mesosphere, and subsequently lost via recombination [see 24]. This is consistent with earlier studies of these effects on [O] in the NCAR TIME-GCM [e.g., 25].

Figure 4 also shows that these systematic differences in MLT [O] are linked to important differences in calculated ionospheric electron densities. Contour plots on the right-hand side of Figure 4 show the daytime (i.e., 12 LT ± 1.5 h in local time) median peak electron densities in the F-region (N_mF_2)

ionosphere as a function of day of year and magnetic latitude, including N_mF_2 observations from the COSMIC satellites [Constellation Observing System for Meteorology, Ionosphere, and Climate satellites, 26]. Both the SD and 4D Tendency nudging approaches of M15, W17, and J18 reproduce the spatiotemporal variability associated with the noontime median N_mF_2 observed by COSMIC, including the 2010 SSW period. However, the direct impact of increased mixing and decreased [O] in the M15 and W17 cases result in low median daytime N_mF_2 values, compared to COSMIC. For example, M15 and W17 simulated maximum median N_mF_2 values never exceed 1.0×10^6 cm^{-3}, whereas COSMIC observed maximum median N_mF_2 exceed 1.5×10^6 cm^{-3} approaching vernal equinox in the equatorial ionization anomaly crests. Although J18 simulated median N_mF_2 values are larger than those simulated by M15 and W17, they are still ~10-30% too low compared to COSMIC observations. Since the zonal mean wind circulation and tidal perturbations in our J18 simulation do not exhibit nudging artifacts around the nudging boundary (and thus less vigorous downward transport), low median N_mF_2 values suggest that [O] is still too low. Additional examination of these simulated low MLT O values in TIME-GCM deserves future consideration, especially given the interplay between dynamics and chemistry at MLT altitudes.

4. CONCLUSIONS

The results presented herein offer an alternative methodology for constraining lower and middle atmospheric dynamics in an upper atmosphere general circulation to the widely-used SD nudging technique called 4D Tendency nudging. Using a set of numerical experiments from the TIME-GCM constrained by NAVGEM-HA horizontal winds and neutral temperatures in the stratosphere and mesosphere, a case study of the 2010 SSW period was performed to gain insight into the differential effects SD and 4D Tendency nudging schemes have on resolving MLT and TI dynamics and composition. At tropical latitudes, important differences in the winds and tides were seen that lead to differences in neutral and ion composition. As a result, it is recommended that the middle and upper atmospheric modeling community strongly consider utilizing 4D Tendency nudging as an option for constraining the dynamical model fields, or at the very least to compliment already implemented SD nudging approaches.

Furthermore, the constraining techniques and analysis presented herein specific to the 2010 SSW period have wider applications. Forecasting space weather driven by SSWs represent a modeling benchmark in Earth system science, because SSWs can be predicted a few days in advance by lower and middle atmosphere forecast systems [e.g., 27]. Thus, any model that seeks to forecast or analyze the short-term variability in the TI system should evaluate the implementation of various nudging techniques and understand the systematic impacts these could have in accurately forecasting [e.g., 6] and or reproducing short-term TI variability.

ACKNOWLEDGEMENTS

This work is the subject of submitted publication [28] in the American Geophysical Union Journal of Advances in Modeling Earth Systems. The co-authors of this work include Douglas P. Drob, David E. Siskind, John P. McCormack, Sarah E. McDonald, and Kenneth F. Dymod of NRL (Code 7630) and Astrid Maute at the NCAR High Altitude Observatory. Additionally, TIME-GCM simulations produced by this work have been used in a recently submitted manuscript to Annales Geophysicae by David E. Siskind [29]. The author is also grateful to Manbharat Dhadly, John Emmert, and Nicholas Pedatella for helpful discussions. Computation resources for this work were provided by the U. S. Department of Defense (DoD) High Performance Computing Modernization Program (HPCMP).

REFERENCES

1. Mendillo, M., H. Rishbeth, R. G. Roble, and J. Wroten (2002), Modelling F_2-layer seasonal trends and day-to-day variability driven by coupling with the lower atmosphere, *Journal of Atmospheric and Solar-Terrestrial Physics, 64(18)*, 1911–1931, doi:http://dx.doi.org/10.1016/S1364-6826(02)00193-1.

2. Liu, H. L. (2016), Variability and predictability of the space environment as related to lower atmosphere forcing, *Space Weather, 14(9)*, 634–658, doi: 10.1002/2016SW001450.

3. SECNAVIST 2400.2A. https://doni.documentservices.dla.mil/secnav.aspx.

4. Marsh, D. R. (2011), Chemical-dynamical coupling in the mesosphere and lower thermosphere, in aeronomy of the earth's atmosphere and ionosphere, in Aeronomy of the Earth's Atmosphere and Ionosphere, IAGA Special Sopron Book Series, vol. 2, edited by M. Abdu and D. Pancheva, pp. 3–17, Springer, Dordrecht, doi:https://doi.org/10.1007/978-94-007-0326-1 1.

5. Pedatella, N. M., T. Fuller-Rowell, H. Wang, H. Jin, Y. Miyoshi, H. Fujiwara, and et al. (2014), The neutral dynamics during the 2009 sudden stratosphere warming simulated by different whole atmosphere models, *Journal of Geophysical Research: Space Physics, 119(2)*, 1306–1324, doi:10.1002/2013JA019421.

6. Smith, A. K., N. M. Pedatella, D. R. Marsh, and T. Matsuo (2017), On the dynamical control of the mesosphere-lower thermosphere by the lower and middle atmosphere*, Journal of the Atmospheric Sciences, 74(3)*, 933–947, doi:10.1175/JAS-D-16-0226.1.

7. Liu, H. L., V. A. Yudin, and R. G. Roble (2013), Day-to-day ionospheric variability due to lower atmosphere perturbations, *Geophysical Research Letters, 40(4),* 665–670, doi:10.1002/grl.50125.

8. Maute, A., M. E. Hagan, V. Yudin, H.-L. Liu, and E. Yizengaw (2015), Causes of the longitudinal differences in the equatorial vertical E × B drift during the 2013 SSW period as simulated by the TIME-GCM, *Journal of Geophysical Research: Space Physics, 120(6)*, 5117–5136, doi:10.1002/2015JA021126.

9. Wang, J. C., L. C. Chang, J. Yue, W. Wang, and D. E. Siskind (2017), The quasi 2-day wave response in TIME-GCM nudged with NOGAPS-ALPHA, *Journal of Geophysical Research: Space Physics, 122(5)*, 5709–5732, doi: 10.1002/2016JA023745.

11. Stauffer, D. R., and N. L. Seaman (1990), Use of four-dimensional data assimilation in a limited-area mesoscale model. Part I: Experiments with synoptic-scale data, *Monthly Weather Review, 118(6)*, 1250–1277, doi:10.1175/1520-0493(1990)118-1250:UOFDDA-2.0.CO;2.

11. Siskind, D. E., D. P. Drob, K. F. Dymond, and J. P. McCormack (2014), Simulations of the effects of vertical transport on the thermosphere and ionosphere using two coupled models, *Journal of Geophysical Research: Space Physics, 119(2)*, 1172–1185, doi:10.1002/2013JA019116.

12. McCormack, J., K. Hoppel, D. Kuhl, R. de Wit, G. Stober, P. Espy, and et al. (2017), Comparison of mesospheric winds from a high-altitude meteorological analysis system and meteor radar observations during the boreal winters of 2009-2010 and 2012-2013, *Journal of Atmospheric and Solar-Terrestrial Physics, 154*, 132 – 166, doi:https://doi.org/10.1016/j.jastp.2016.12.007.

13. Roble, R. G., and E. C. Ridley (1994), A thermosphere-ionosphere-mesosphere-electrodynamics

general circulation model (time-GCM): Equinox solar cycle minimum simulations (30-500 km), *Geophysical Research Letters, 21 (6),* 417-420, doi:10.1029/93GL03391.

14. Solomon, S. C., and L. Qian (2005), Solar extreme-ultraviolet irradiance for general circulation models, *Journal of Geophysical Research: Space Physics, 110(A10),* doi:10.1029/2005JA011160.

15. Richmond, A. D., and A. Maute (2014), Ionospheric Electrodynamics Modeling, chap. 6, pp. 57{71, American Geophysical Union (AGU), doi: 10.1002/9781118704417.ch6.

16. Lindzen, R. S. (1981), Turbulence and stress owing to gravity wave and tidal breakdown, *Journal of Geophysical Research Oceans, 86(C10)*, 9707{9714, doi:10.1029/JC086iC10p09707.

17. Hagan, M. E., and J. M. Forbes (2002), Migrating and nonmigrating diurnal tides in the middle and upper atmosphere excited by tropospheric latent heat release, *Journal of Geophysical Research: Atmospheres, 107 (D24)*, ACL 6-1-ACL 6-15,doi:10.1029/2001JD001236.

18. Hagan, M. E., and J. M. Forbes (2003), Migrating and nonmigrating semidiurnal tides in the upper atmosphere excited by tropospheric latent heat release*, Journal of Geophysical Research: Space Physics, 108 (A2)*, doi:10.1029/2002JA009466.

19. Eckermann, S. D., K. W. Hoppel, L. Coy, J. P. McCormack, D. E. Siskind, K. Nielsen, and et al. (2009), High-altitude data assimilation system experiments for the northern summer mesosphere season of 2007*, Journal of Atmospheric and Solar-Terrestrial Physics, 71 (3),* 531-551, doi: https://doi.org/10.1016/j.jastp.2008.09.036, global Perspectives on the Aeronomy of the Summer Mesopause Region.

20. Jeuken, A. B. M., P. C. Siegmund, L. C. Heijboer, J. Feichter, and L. Bengtsson (1996), On the potential of assimilating meteorological analyses in a global climate model for the purpose of model validation, *Journal of Geophysical Research: Atmospheres, 101 (D12),* 16,939{16,950, doi:10.1029/96JD01218.

21. Forbes, J. M., and R. A. Vincent (1989), Effects of mean winds and dissipation on the diurnal propagating tide: An analytic approach, *Planetary and Space Science, 37(2),* 197–209, doi:https://doi.org/10.1016/0032-0633(89)90007-X.

22. Yamazaki, Y., and A. D. Richmond (2013), A theory of ionospheric response to upward-propagating tides: Electrodynamic effects and tidal mixing effects, *Journal of Geophysical Research Space Physics, 118(9*), 5891–5905, doi:10.1002/jgra.50487.

23. Fuller-Rowell, T., H. Wang, R. Akmaev, F. Wu, T.-W. Fang, M. Iredell, and A. Richmond (2011), Forecasting the dynamic and electrodynamic response to the January 2009 sudden stratospheric warming, *Geophysical Research. Letters*, *38*, L13102, doi: 10.1029/2011GL047732.

24. Forbes, J. M., R. G. Roble, and C. G. Fesen (1993), Acceleration, heating, and com- positional mixing of the thermosphere due to upward propagating tides, *Journal of Geophysical Research: Space Physics, 98(A1),* 311–321, doi:10.1029/92JA00442.

25. Jones, M., J. M. Forbes, and M. E. Hagan (2014), Tidal-induced net transport effects on the oxygen distribution in the thermosphere, *Geophysical Research Letters, 41(14),* 5272–5279, doi:10.1002/2014GL060698.

26. Anthes, R. A., P. A. Bernhardt, Y. Chen, L. Cucurull, K. F. Dymond, D. Ector, and et al. (2008), The COSMIC/FORMOSAT-3 Mission: Early Results, *Bulletin of the American Meteorological Society, 89(3)*, 313–334, doi:10.1175/BAMS-89-3-313.

27. Kim, Y.-J., and M. Flatau (2010), Hindcasting the January 2009 arctic sud- den stratospheric warming and its influence on the arctic oscillation with unified parameterization of orographic drag in NOGAPS. Part I: Extended- range stand-alone forecast, *Weather and Forecasting, 25(6),* 1628–1644, doi: 10.1175/2010WAF2222421.1.

28. Jones Jr., M., D. Drob, D. Siskind, J. McCormack, A. Maute, S. McDonald, and K. Dymond (2018), Evaluating different techniques for constraining lower atmospheric variability in an upper atmosphere general circulation model: A case study during the 2010 sudden stratospheric warming, *Journal of Advances in Modeling Earth Systems* (under review).

29. Siskind, D. E., Jones Jr., M., J., Drob, D. P., McCormack, J. P., Hervig, M. E., Marsh, D. R., Mlynczak, M. G., Bailey, S. M., Maute, A., and Mitchell, N. J. (2018), On the relative roles of dynamics and chemistry governing the abundance and diurnal variation of low latitude thermospheric nitric oxide, *Annales Geophysicae*, https://doi.org/10.5194/angeo-2018-112 (under review).